100 Hz–10 kHz Bottom Backscattering Model: Generalized Treatment of Sediment Sound Propagation, Sediment Volume Scattering, and Interface-Roughness Scattering

by Darrell R. Jackson, Paul D. Ingalls, and Kou-Ying Moravan

Technical Memorandum
APL-UW TM 1-94
April 1994

Applied Physics Laboratory University of Washington
1013 NE 40th Street Seattle, Washington 98105-6698

Contract N00039-91-C-0072

100 Hz–10 kHz Bottom Backscattering Model: Generalized Treatment of Sediment Sound Propagation, Sediment Volume Scattering, and Interface-Roughness Scattering

by Darrell R. Jackson, Paul D. Ingalls, and Kou-Ying Moravan

Technical Memorandum
APL-UW TM1-94
April 1994

Applied Physics Laboratory University of Washington
1013 NE 40th Street Seattle, Washington 98105-6698

Contract N00039-91-C-0072

Acknowledgment

This work was sponsored by the ONR-AEAS Program.

Abstract

A model for bottom backscattering strength in the frequency range 100 Hz to 10 kHz is presented. This model generalizes an earlier low-frequency model intended for the smaller frequency range 100–1000 Hz. The new model matches the predictions of an existing high-frequency model (10–100 kHz) but offers new insights into the effect of fine-scale layering. Scattering from both sediment volume inhomogeneity and interface roughness is included in the model. For silt and clay sediments, sediment volume scattering is usually the dominant process. The model requires profile functions for average sound speed, mass density, sound absorption, and volume scattering strength in the sediment. In addition, two parameters describing the spectrum of interface roughness are required. Use of the small-roughness perturbation approximation prevents application of the model to extremely rough bottoms (e.g., gravel and rock).

Preliminary comparisons with data show that the model can reproduce an interesting frequency dependence often seen in bottom backscattering. This includes a decrease in scattering strength with increasing frequency in the 100–1000 Hz range, an increase as frequency approaches 10 kHz, and approximate constancy or a slow rise above 10 kHz. The increase in sound speed with depth typically observed in sediments causes upward refraction which, in some cases, leads to enhancements of scattering by 6–8 dB.

Contents

List of Figures

1 INTRODUCTION

This report describes a model for bottom acoustic backscattering in the frequency range 100 Hz to 10 kHz. This model is a generalization of a model covering the low-frequency range 100 Hz to 1 kHz [1, 2]. The older, low-frequency model was itself an adaptation of a high-frequency model covering the frequency range 10–100 kHz [3]. The present work bridges the 1–10 kHz gap between the low-frequency and high-frequency regimes in a manner consistent with data and with both of the older models. Rather than making phenomenological modifications to the older model, we have generalized it to embody both large- and small-scale environmental features. This more general model contains the older models as limiting cases, but also allows more realistic modeling of bottom acoustic properties.

Like the earlier models, the present model predicts bottom scattering strength in terms of sediment acoustic properties (including volume scattering) and parameters for interface roughness. Earlier model/data comparisons have shown that sediment volume scattering is a major contributor to bottom backscattering [2, 4, 5], and it is a major part of the present work. In the high-frequency model, sediment volume scattering is treated in an approximation in which gradients in average sound speed, absorption, and mass density are neglected. The resulting bottom scattering strength is almost independent of frequency, provided certain assumptions (to be discussed later) are made. This is in agreement with available high-frequency data for mud bottoms [4, 5, 6] where sediment volume scattering is expected to dominate scattering due to interface roughness. In the low-frequency model, average sound speed increases with depth in the bottom on scales of 10–100 m. The resulting upward refraction has strong effects in scattering predictions. The most important refractive effect is focusing with an attendant increase in scattering strength. Figure 1 shows this increase in bottom scattering strength for frequencies below 1000 Hz, an effect that is often observed in real data. Wideband data often exhibit a U-shaped curve of scattering strength vs frequency, with scattering strength showing a minimum somewhere between 1 kHz and 5 kHz. This minimum is above the frequency range of the low-frequency model, but if the model is used in this range, it produces a flat curve as illustrated in Fig. 1.

Although the high-frequency model ignored gradients in sediment properties, there is little doubt that gradients are relevant at high frequencies as well. In fact, the high-frequency model uses *adjusted* values of sediment sound speed and density [3] to partially account for the steep gradients in the upper few centimeters of the bottom, where there is a tendency for sediment properties to approach those of water. The approach we take in the present work is to allow more general profiles of sediment acoustic properties with gradients on both small scales and large scales. In this approach, the transition between low- and high-frequency models occurs naturally.

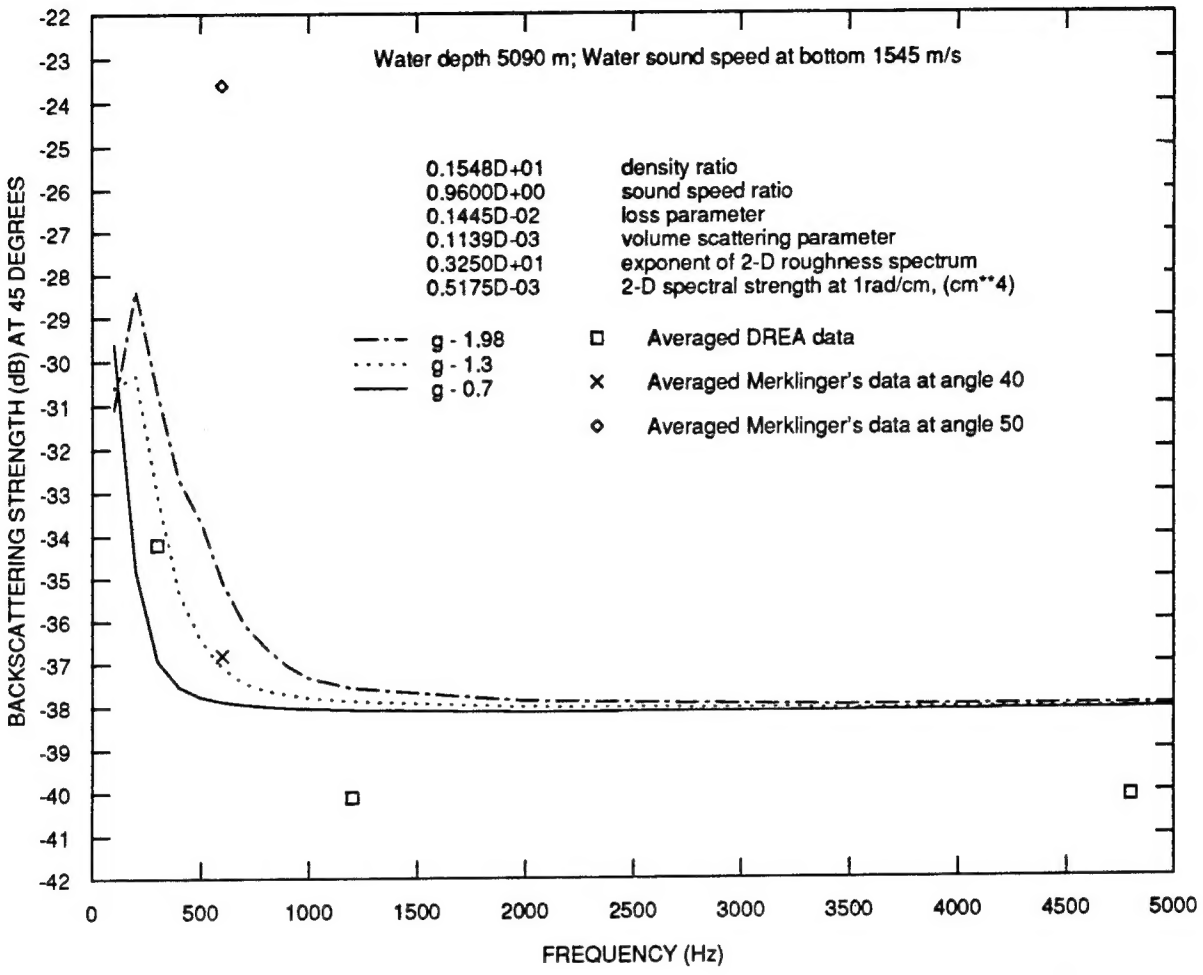

Fig. 1. Frequency dependence of low-frequency model at a grazing angle of 45° compared with historical data. Three values of the initial sound speed gradient, g, are used. As the gradient is reduced, the model curve flattens and becomes approximately independent of frequency.

Figure 2 shows typical sound-speed profiles employed in the low- and high-frequency models, along with a more realistic profile. The term "realistic" should not be interpreted to mean "typical," as there is great variety in the geological structure of the ocean bottom. The more realistic profile of Fig. 2 includes a slow upper layer about 10 cm thick. The upper 5–20 cm of the bottom is often a region of strong mixing due to bioturbation (animal activity) and hydrodynamic activity, which can loosen fine sediments. As mentioned earlier, the effects of this layer were approximated in the high-frequency model by the simple expedient of reducing sediment sound speed and density relative to conventional values obtained, for example, from

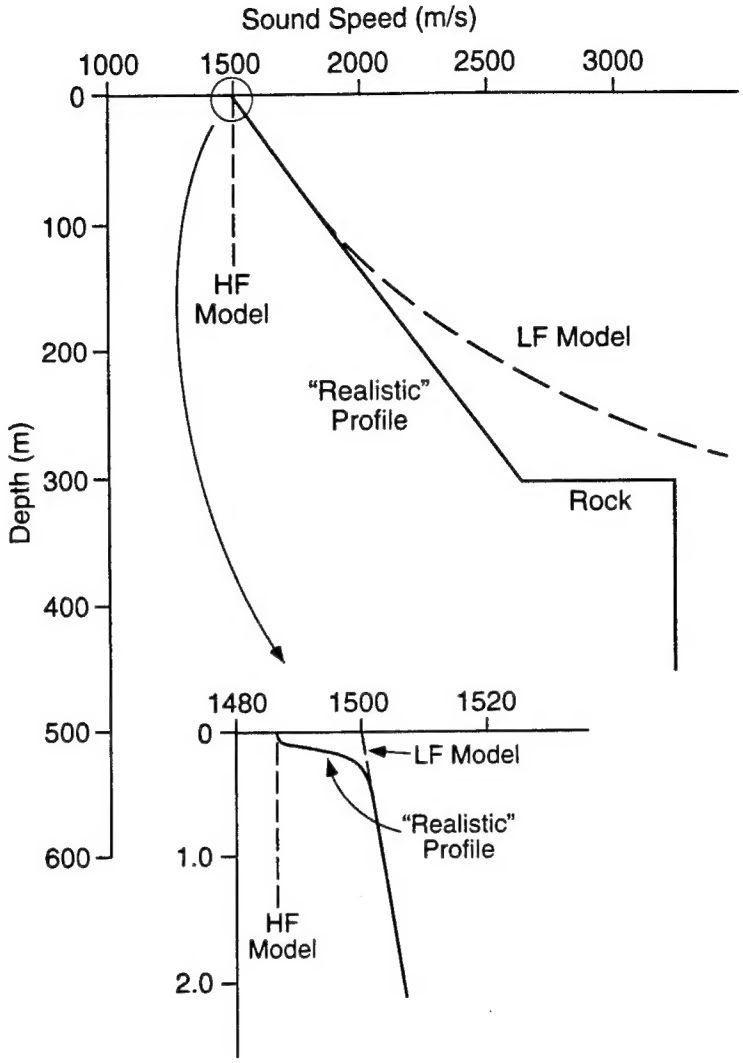

Fig. 2. Idealized bottom sound speed profiles (dashed curves) employed in the high-frequency and low-frequency models compared with a more realistic profile (solid curve). The sediment begins at zero depth. The water sound speed (not shown) may be slightly larger or smaller than the surficial value of sediment sound speed.

the Hamilton-Bachman regression relations [7]. The adjusted values were taken to be independent of depth on the assumption that acoustic penetration would not exceed the depth of the upper layer. Deeper in the sediment, sound speed increases owing to consolidation. In the older low-frequency model, this increase is gradual near the interface (typically about 1 m/s per meter of depth), but accelerates and becomes singular at finite depth. More realistically, the sound speed at depth would

not increase past the value expected for fully consolidated sediment (e.g., mudstone) or for rock (about 2000–6500 m/s) [8]. Thus, a more realistic sound-speed profile, as indicated in Fig. 2, includes a 5- to 20-cm-thick slow layer near the interface, and then increases with depth on a scale of order 100 m, finally reaching a maximum value. In the region where the maximum sound speed is attained, the bottom material is fully consolidated sediment or rock and it can support shear waves. Our present model still does not treat shear effects, which are most likely to be important only when the sediment cover is thin or the frequency is very low. Unconsolidated sediments do support shear waves, but shear effects are expected to be very small in this case [9].

The generalized model solves a problem arising from the artificial nature of the sound speed profile in the older low-frequency model. In that model, the sound speed profile becomes singular (infinite) at a finite depth in the sediment. While this singularity is usually below the penetration depth of acoustic energy, it sometimes is not, particularly for steep grazing angles and at the low frequencies near 100 Hz. Mourad and Jackson [2] have noted that this singularity causes an unusually strong oscillation in the bottom scattering strength at large grazing angles. Such oscillations are an expected consequence of the refracted up-going wave, but the singularity gives an unrealistically large amplitude for the up-going wave at large grazing angles. This large-amplitude up-going wave also causes a relatively steep increase in scattering strength at the larger grazing angles (roughly, 45° to 85°). It will be seen that this steep increase is absent with more realistic profiles.

This report is organized as follows. Section 2 treats propagation of sound in the bottom and volume scattering from scatterers or inhomogeneities embedded in the bottom sediment. It is mainly this portion of the model that is significantly improved relative to earlier versions, but there is also a related improvement in the treatment of scattering from interface roughness. The volume-scattering component of the model is illustrated in Section 2 by several numerical examples. Section 3 gives a brief account of the interface roughness scattering portion of the model, which has been generalized to include effects of gradients in the sediment. These effects are also illustrated by numerical examples. Section 4 comments upon the combined model for bottom backscattering and discusses dimensionless sediment profile functions. Finally, conclusions and recommendations for future work are given in Section 5.

2 BOTTOM PROPAGATION, REFLECTION, AND VOLUME SCATTERING

A description of propagation in a stratified ocean bottom is required for computing both sediment volume scattering and interface roughness scattering. The earlier low-frequency model [1, 2] employed a linear profile for the squared wavenumber, which is specific to Airy-function solutions. The main changes in the present model with respect to this earlier work are as follows:

1. The wave equation is now solved by a general numerical technique for smooth profiles of sediment properties, rather than for the specific case having an Airy-function result. This allows sediment profiles to be less specific than before, yet still allows checks against specific prior results.

2. Density-gradient effects are treated.

3. Complex reflection coefficient values are no longer inconsistent with the evaluation of sediment propagation. This improves upon the Rayleigh impedance-mismatch reflection coefficient, which is strictly appropriate only for a semi-infinite sediment of depth-independent properties.

4. Volume scattering and absorption within the ocean bottom are depth dependent.

2.1 Bottom Propagation

Consider horizontally stratified (fluid) bottom sediments in contact with isovelocity seawater at a horizontal interface. Shear waves are not treated here. The sediment properties of sound speed, absorption, and density $\rho(z)$ may vary with the vertical coordinate z in the sediments. In this case [10] the field that obeys the wave equation, and (for a given acoustic frequency) also the Helmholtz equation, is not the acoustic pressure p, but rather $p/\sqrt{\rho}$.

For incident plane waves of frequency f and grazing angle θ, the separation-of-variables technique yields

$$p(x,z,t)/\sqrt{\rho(z)} = X(x)Z(z)e^{-i2\pi ft} \; ; \tag{1}$$

then fix the value of a θ-dependent separation constant k_x^2 and solve the remaining Helmholtz equation for the z-dependent factor $Z(z)$. That is

$$X''(x) + k_x^2 X(x) = 0 \; , \tag{2}$$

$$X(x) = e^{ik_x x} \; , \tag{3}$$

and

$$Z''(z) + K_z^2(z)Z(z) = 0\ . \tag{4}$$

The squared wavenumber field needed for the latter equation is then

$$K_z^2(z) = k^2(z) - k_x^2 + \frac{1}{2}\rho''(z)/\rho(z) - \frac{3}{4}[\rho'(z)/\rho(z)]^2, \tag{5}$$

with

$$k_x = 2\pi f \cos\theta \ / \ c_w\ . \tag{6}$$

Here the z-independent constant k_x is the (real) horizontal component of the wavenumber, conveniently evaluated here at $z = 0+$ (the sediment-water interface is at $z = 0$). The sound speed in water is denoted c_w, and $k^2(z)$ is the (complex) squared wavenumber in the sediment. The imaginary part of $k(z)$ allows for absorption of sound in the sediment. The density terms that are included here were developed elsewhere [10]. It is implicit in Eq. (5) that profiles of sound speed and absorption are available (to construct $k^2(z)$) and that profiles of density and its first two derivatives are also available.

The second-order Helmholtz equation for the complex function $Z(z)$ is obtained numerically by solving the equivalent set of four coupled first-order ordinary differential equations obeyed by functions that represent the separated real and imaginary parts of $Z(z)$ and $Z'(z)$ [11]. After normalizing $Z(z)$ for a plane incident sound wave for which $p/\sqrt{\rho}$ has unit amplitude, the bottom backscattering differential cross section per unit area and per unit solid angle is given by the following integration over the volume scatterers [1, 2]:

$$\sigma_{bv}(\theta) \ = \ \int_0^\infty dz\ \sigma_v(z)\ |Z(z)|^4. \tag{7}$$

The bottom scattering strength as conventionally defined is

$$BSSV \ = \ 10\ \log_{10}\ \sigma_{bv}(\theta), \tag{8}$$

where the V indicates that we are considering only the contribution of sediment volume scattering to the bottom scattering strength. In Eq. (7), $\sigma_v(z)$ is the volume-specific differential scattering cross section for the sediments, i.e., $10\ \log_{10}\ \sigma_v(z)$ is the "volume scattering strength" [12].

2.2 Numerical Solution

The numerical solution proceeds upward to the water/sediment interface from a chosen starting depth in the sediment. Initial values for Z and Z' at the starting

depth are chosen consistent with the tunneling or oscillatory character of $Z(z)$ there, that is, the negative or positive sign of the real part of K_z^2, respectively.

For the usual case where relatively small grazing angles are of interest, an increasing sediment sound speed produces a turning point (or vertex) in the raytracing limit. The corresponding wave solution is exponentially small below the turning point depth. In wave theory, this is the depth below which the real part of K_z^2 is negative. An unnormalized wave solution having arbitrary amplitude is started from well into this evanescent region as for a decaying exponential, so that derivative and value are connected according to

$$Z'/Z = |K_z| \, . \tag{9}$$

The amplitude of this wave is fixed by a normalization procedure defined below.

In steep-angle cases, rays need never vertex, but can instead continue to arbitrarily great depths and eventual absorption. The wave solution is then an entirely downward-directed field at depths below all changes in sediment properties. Then the solution is started as for a traveling wave, so that

$$Z'/Z = -i \, |K_z| \, . \tag{10}$$

In all cases the integration proceeds upward from the starting depth until the water/sediment interface is reached. There the solution is normalized by forcing continuity across the interface for both the acoustic pressure $p(z) = Z(z) \sqrt{\rho(z)}$ and the z-derivative quantity $p'(z)/\rho(z)$.

The complex reflection coefficient for the water/sediment interface is the ratio of upward and downward wave amplitudes in the wave solution on the water side of the interface. In this wave-theory treatment, the reflection coefficient depends strongly on angle and frequency, unlike the simpler Rayleigh impedance-mismatch reflection coefficient appropriate to a uniform sediment having depth-independent sound speed and density. These improved values for the reflection coefficient apply even in the Airy-function (k^2-linear-profile) limit. This improvement influences estimates of scattering by interface roughness, which is sensitive to the relative amplitudes of upward-directed and downward-directed fields at the interface-roughness scatterers. As will be seen in the following section, the influence on interface scattering can be very strong.

The normalized wave solution is obtained after jumping the wave solution into the water across the water/sediment interface and renormalizing for unit amplitude of the downward-directed incident plane-wave component of the wave solution above the sediment. In the water above $z = 0$, let

$$Z(z) = De^{+ik_z z} + Ue^{-ik_z z} \, , \tag{11}$$

with

$$k_z = -2\pi f \sin\theta \; / \; c_w \; . \tag{12}$$

Approaching $z = 0$ from the water side, we then have

$$(Z'/Z)_{0+} = ik_z \frac{D - U}{D + U} \; . \tag{13}$$

The complex reflection coefficient is just

$$R(\theta) = U/D = \frac{ik_z - (Z'/Z)_{0+}}{ik_z + (Z'/Z)_{0+}} \; . \tag{14}$$

In the evaluation of roughness scattering, the above result also simplifies the following expression that appears in the roughness-scattering portion of the model. We note that the normalized admittance presented by the interface to a plane acoustic wave is

$$\frac{1 - R(\theta)}{1 + R(\theta)} = \frac{(Z'/Z)_{0+}}{ik_z} \; . \tag{15}$$

The unnormalized solution is just divided everywhere by the complex amplitude D of its downgoing component in the water to produce the normalized $Z(z)$ solution for unit incident-wave amplitude. This normalization step is not needed for the complex reflection coefficient U/D, but it is needed for sediment scattering-strength integrals.

Bottom reflection loss is given by

$$BRL = -20 \; \log_{10} \; |U/D| \; . \tag{16}$$

This is a positive decibel equivalent of the complex reflection coefficient and is shown along with the scattering strength $BSSV$ in some of the examples that follow.

The following examples illustrate some of the features of the generalized treatment of sediment volume scattering. Low-frequency examples are considered for the most part, as propagation effects are most obvious below about 1 kHz. It is important to note, however, that the generality of the model makes it possible to treat the effects of sediment layering at both large and small scales, and hence at both low and high frequencies. Figure 3 gives the sound speed profiles used in the following examples.

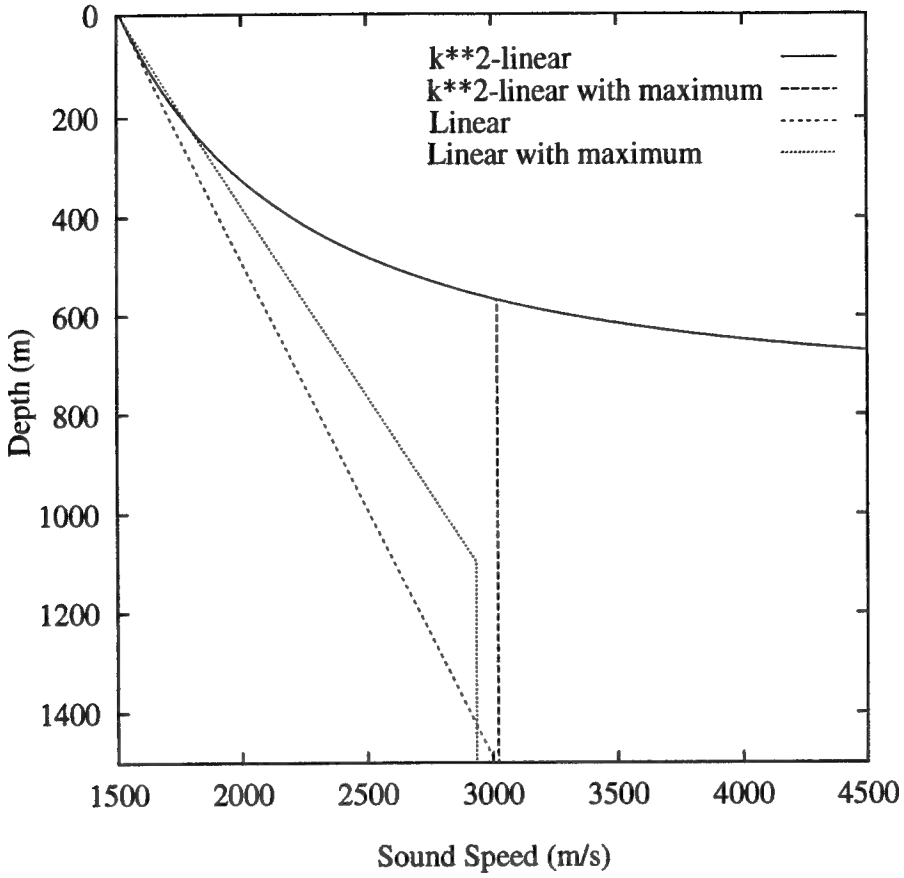

Fig. 3. Sediment sound speed profiles used in illustrative examples.

2.3 k^2-Linear Profile

Figures 4 and 5 show calculations of $BSSV$ (from sediment volume scattering only—no roughness) that check known cases from prior work, except that the wave solution is now obtained by a more general numerical technique. In this prior work, $k^2(z)$ was taken to have a linear dependence on depth [1, 2], for which the field $Z(z)$ is given by an Airy function. The parameters and profile functions appropriate to a comparison with Mourad and Jackson are

$$\begin{aligned} \text{Frequency, } f &= 500 \text{ Hz and } 100 \text{ Hz} \\ \text{Water sound speed, } c_w &= 1530.0 \text{ m/s} \\ \text{Surficial sediment sound speed, } c_1 &= 1510.11 \text{ m/s} = c_w \times\ 0.987 \\ \text{Initial slope of sound speed profile, } |dc/dz|_0 &= 1.0 \text{ s}^{-1} \\ \text{Loss parameter, } \delta &= 0.00164 \end{aligned}$$

$$
\begin{aligned}
\text{Squared wavenumber, } k^2(z) &= k_1^2\,(1+i\delta)^2\,(1-z/z_{\text{wall}}) \\
\text{Real part of surficial wavenumber, } k_1 &= 2\pi f/c_1 \\
\text{Depth of singularity, } z_{\text{wall}} &= -755.1 \text{ m} \\
\text{Mass density, } \rho &= 1.72 \times 1026 \text{ kg/m}^3 \\
\text{Absorption coefficient, } \alpha_1 &= 40\pi\delta f \,/\, (\, c_1 \,\ln(10)\,) \\
\text{Volume scattering parameter, } \sigma_2 &= 0.0002 \\
\text{Sediment volume scattering strength, } \sigma_v &= \alpha_1\,\sigma_2\,.
\end{aligned}
$$

The parameter z_{wall} is the depth at which the sound speed becomes infinite for this special profile. It is not an independent parameter and can be found in terms of c_1 and $|dc/dz|_0$. The parameter α_1 is the sound absorption coefficient (in decibels/unit length) just below the sediment/water interface, and σ_2 [1, 2, 3] is a convenient dimensionless form for the volume scattering strength, as discussed in Section 4. The parameters and results here are the same as those in prior calculations

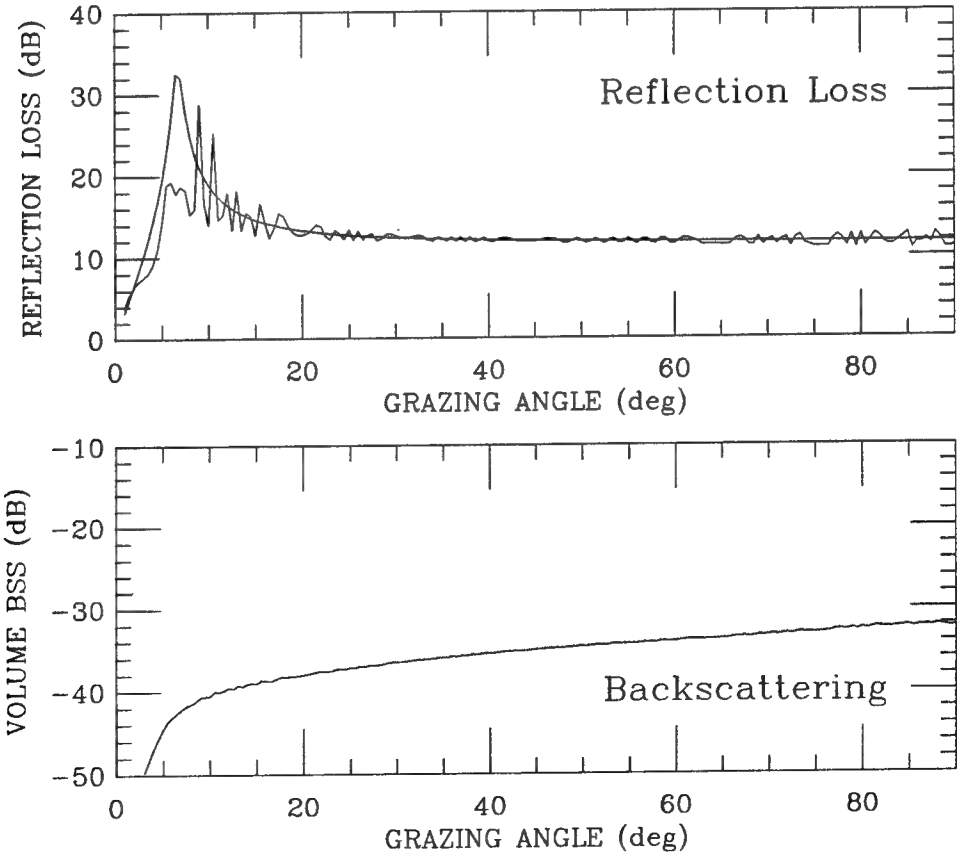

Fig. 4. Model curves for reflection loss and backscattering strength at 500 Hz for a linear dependence of squared wavenumber on depth (k^2-linear case). The smooth reflection loss curve is computed for the gradient-free case.

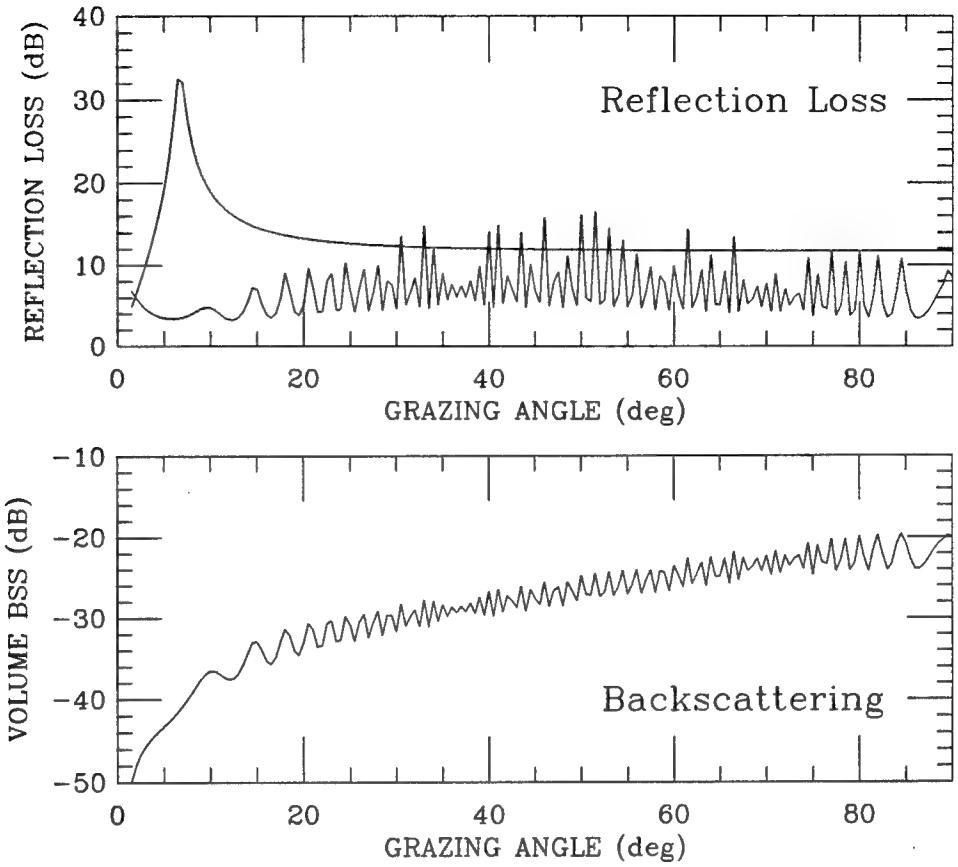

Fig. 5. As in Fig. 4 except the frequency is 100 Hz.

for this Airy-function case (see Fig. 3 of Ref. 2). This is a significant check of the present numerical methods. The 500-Hz *BSSV* values show little of the oscillatory interference structure vs grazing angle that is so apparent at 100 Hz (see Fig. 4). This effect comes from the higher sound absorption at the higher frequency and the consequently weaker upward-directed wave reflecting off the deep barrier in the sediment. The absorption of sound at 100 Hz is so low that interference of the upward and downward waves in the sediment is important [2].

Also shown with Figs. 4 and 5 are the corresponding values for bottom reflection loss, *BRL*, and the smooth, frequency-independent Rayleigh values calculated from the impedance mismatch at the interface between sediment and water. The *BRL* curves emphasize the phenomena that have arisen at low frequencies as a result of the combination of upward refraction and small absorption. The 500-Hz results of Fig. 4 show that for most angles *BRL* can be approximated by the Rayleigh reflection coefficient computed from the impedance mismatch. The deepest sediments are not

important when sound absorption is high. The 100-Hz results of Fig. 5, however, show the systematically lower reflection losses that correspond to low-frequency sound reaching and returning from deep sediments. Comparing the peaks in *BSSV* and *BRL* shows an obvious correlation between high *BSSV* and high *BRL*. That is, greater sediment backscattering goes hand in hand with greater penetration of sound into the sediments below the interface. Deep sediments are important, and different possible treatments of them are distinguishable at low frequencies.

2.4 k^2-Linear Profile with Maximum Sound Speed

Figure 6 shows the effect of clipping the sound speed at a maximum value rather than letting it become infinite at $z = z_{\text{wall}}$ and then imaginary at greater depths, as it does for the Airy-function limit. The parameters for the calculations in Fig. 6 are the same as those for the 100-Hz calculations of Fig. 5, except that for

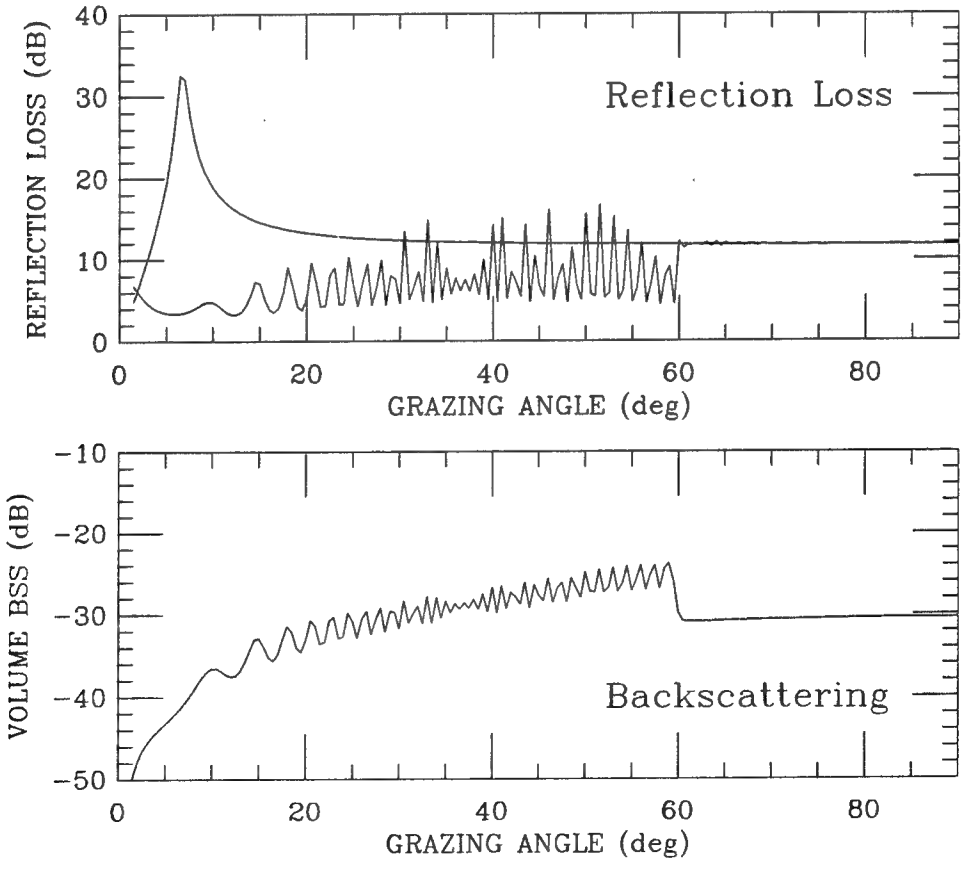

Fig. 6. As in Fig. 5 except the sound speed was held constant at depths greater than the depth at which it is twice the surficial value.

these calculations the sediment sound speed was only allowed to double in value with increasing depth. At greater depths, it was then held constant. Near 90° grazing angle, these low-frequency results are quite different from the Airy case, as expected from the fact that rays would no longer vertex at an unphysical barrier but would instead continue deeper and deeper until absorbed. With the absence of an upward wave reflected off the deep barrier at such steep incidence, the interference character in *BSSV* has disappeared. The impedance-mismatch values for *BRL* have also become a good approximation. At shallower angles, however, the unclipped profile does very well, giving essentially identical results (compare Figs. 5 and 6). This also accords with ray theory, since rays can only reach the changed part of the sediment profile for the steepest grazing angles. The most striking feature of Fig. 6 is the approximately 6-dB drop in *BSSV* for the steep grazing angles where there is no upward-refracted wave. While this is not a very realistic situation, it illustrates the strong scattering enhancements that occur as a result of upward waves. From a ray viewpoint, this enhancement corresponds to superposition of the four round-trip multipath combinations provided by upward refraction. This can give a 6-dB effect, although the upward-refracted wave increases average sound intensity at the volume scatterers by 3 dB at most (when the amplitude of the upward wave is comparable to that of the downward wave).

At higher frequencies, even near-vertical backscattering is not sensitive to the presence or absence of a barrier at $z = z_{\text{wall}}$ (e.g., see Fig. 4). The higher sound absorption makes deep-sediment details irrelevant. The sediments near the water interface then dominate.

2.5 Linear Sound Speed Profile

Figure 7 shows 100-Hz *BSSV* calculations for a linear sound-speed profile. Here, the slope of the linear profile is the same as the initial slope in the linear-k^2 Airy case of Fig. 5, which corresponded to infinite sound speed 755.1 m into the sediment. An important difference between these cases is that different amounts of the sediment are strongly ensonified. In particular, the linear-$c(z)$ case does not have an unphysical barrier for vertical ensonification. Parameters and profile functions used for Fig. 7 were

$$\begin{aligned}
\text{Frequency, } f &= 100 \text{ Hz} \\
\text{Water sound speed, } c_w &= 1530.0 \text{ m/s} \\
\text{Surficial sediment sound speed, } c_1 &= 1510.11 \text{ m/s} = c_w \times 0.987 \\
\text{Slope of sound speed profile, } |dc/dz| &= 1.0 \text{ s}^{-1} \\
\text{Loss parameter, } \delta &= 0.00164 \\
\text{Squared wavenumber, } k^2(z) &= k_1^2 \, (1 + i\delta)^2 \; / \; (1 + z/z_{\text{ref}})^2 \\
\text{Real part of surficial wavenumber, } k_1 &= 2\pi f / c_1
\end{aligned}$$

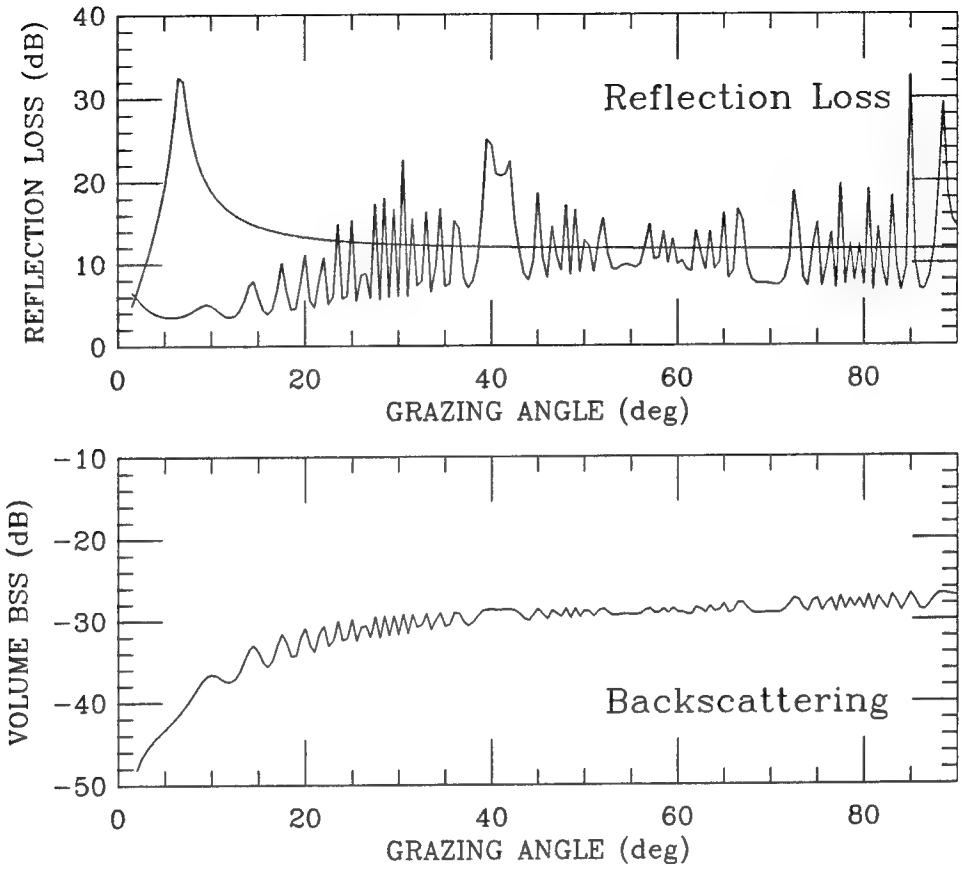

Fig. 7. As in Fig. 5 except the sound speed (rather than squared wavenumber) varies linearly with depth.

$$\begin{aligned} \text{Reference depth, } z_{\text{ref}} &= -1510.2 \text{ m} \\ \text{Mass density, } \rho &= 1.72 \times 1026 \text{ kg/m}^3 \\ \text{Volume scattering parameter, } \sigma_2 &= 0.0002 \ . \end{aligned}$$

The volume scattering strength is derived from the dimensionless parameter σ_2 as in the previous examples. The parameter z_{ref} determines the slope of the sound speed profile. The low-angle $BSSV$ results for the linear-$c(z)$ case of Fig. 7 are similar to the low-angle results in the Airy case of Fig. 5. However, the steeper angles show a systematic difference, as might be expected from a raytracing viewpoint. Once again, the deep details of the sediments have become significant at this low frequency. Absence of the "wall" has reduced the magnitude of the oscillations in $BSSV$ as a function of grazing angle and has reduced the scattering strength at angles greater than about 40°.

2.6 Linear Sound Speed Profile with Maximum Sound Speed

Figure 8 shows results calculated for yet another shape of the $c(z)$ sound-speed profile. The sound speed profile, $c(z)$, is again linear but is now held constant starting at the depth of a basement under the sediment. This case was motivated by a published sediment raytracing example for a site in the Caribbean Sea (see Fig. 8 of Ref. 13). Absorption and maximum sound speed were treated as in the prior examples above, but with the altered numerical values shown below. Otherwise, values were chosen to be similar to the raytracing example cited.

$$\begin{aligned} \text{Frequency, } f &= 100 \text{ Hz} \\ \text{Water sound speed, } c_w &= 1547.79 \text{ m/s} \\ \text{Surficial sediment sound speed, } c_1 &= 1508.17 \text{ m/s} = c_w \times 0.9744 \\ \text{Slope of sound speed profile, } |dc/dz| &= 1.3 \text{ s}^{-1} \\ \text{Loss parameter, } \delta &= 0.0015 \end{aligned}$$

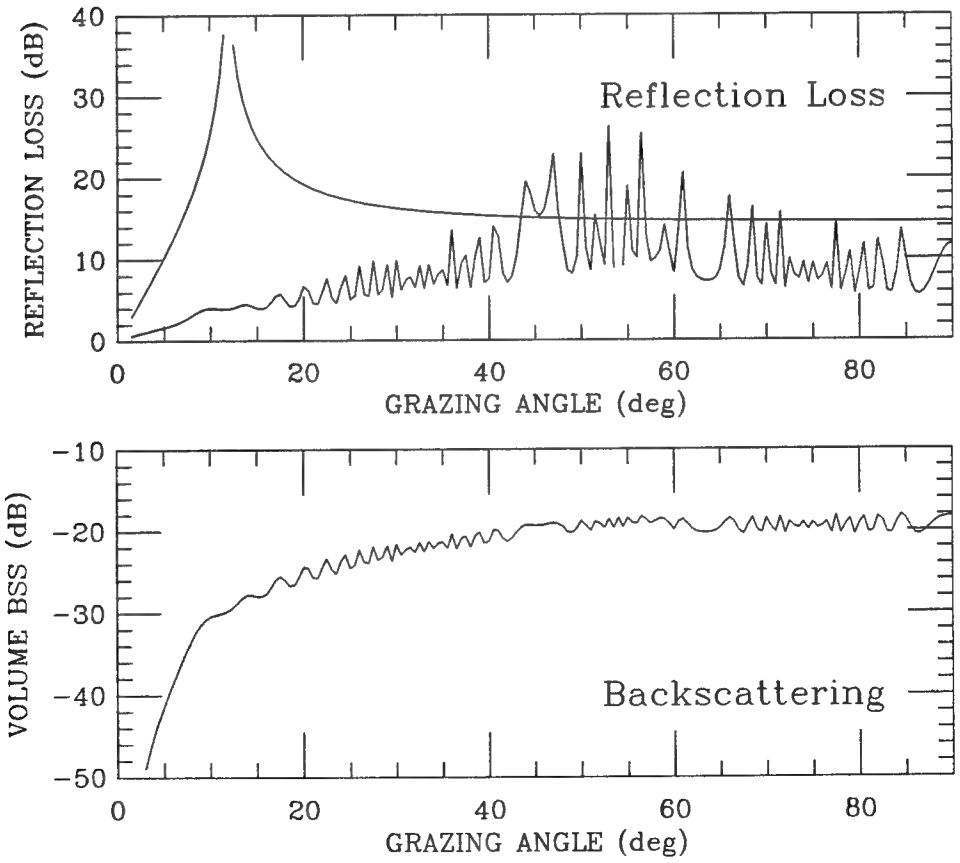

Fig. 8. Model curves for reflection loss and backscattering strength for a linear sound-speed profile with a constant-speed basement. The frequency is 100 Hz.

$$
\begin{aligned}
\text{Squared wavenumber, } k^2(z) &= k_1^2\,(1+i\delta)^2 \,/\, (1+z/z_{\text{ref}})^2 \\
&\quad (\text{for } z \text{ above } z_{\text{base}}) \\
\text{Real part of surficial wavenumber, } k_1 &= 2\pi f/c_1 \\
\text{Reference depth, } z_{\text{ref}} &= -1160.1 \text{ m} \\
\text{Basement depth, } z_{\text{base}} &= -1097.2 \text{ m} = -600 \text{ fathoms} \\
\text{Mass density, } \rho &= 1.5 \times 1026 \text{ kg/m}^3 \\
\text{Volume scattering parameter, } \sigma_2 &= 0.001\ .
\end{aligned}
$$

The volume scattering strength is derived from the dimensionless parameter σ_2 as in the previous examples.

2.7 Frequency Dependence Due to Strongly Scattering Upper Sediment

Figure 9 shows total BSS values for several provinces from the Geddes compilation of historical data [14]. The figure gives backscattering strength vs frequency for a grazing angle of 45°. These experimental results for backscattering have a U-shaped frequency dependence, with the minimum backscattering in our frequency range. This U shape is seen in the data from several but not all of the provinces in Ref. 14.

To generate such an effect in the simplest possible way, it was found sufficient to increase the volume scattering parameter σ_2 for a thin upper portion of the seabed sediments, without giving its value any frequency dependence or a more detailed profile function. The model then yields a fall and a rise in backscattering arising naturally from the frequency dependence in the absorption loss (constant δ vs frequency). Two competing effects account for this. First, absorption rises linearly with frequency for a frequency-independent δ value, so that $BSSV$ values initially fall with increasing frequency owing to supression of the upgoing wave. (The δ constant is a conversion factor giving the imaginary part of the wavenumber from the real part, which rises with frequency, so that absorption also rises.) The thin upper sediment layer is almost irrelevant at low frequencies because the depth of ensonification is much greater than the layer thickness. As the frequency increases, the upper sediment layer becomes important compared with the deeper sediment as increased absorption reduces the depth of penetration, so that upper-sediment scattering controls the $BSSV$ values at high frequencies. Finally, at frequencies such that the penetration depth is smaller than the layer thickness, $BSSV$ becomes frequency independent as the linear increase in volume scattering strength with frequency (dictated by the relation given earlier between the volume scattering strength σ_v and the dimensionless, frequency-independent parameter σ_2) offsets the inverse frequency dependence of the penetration depth.

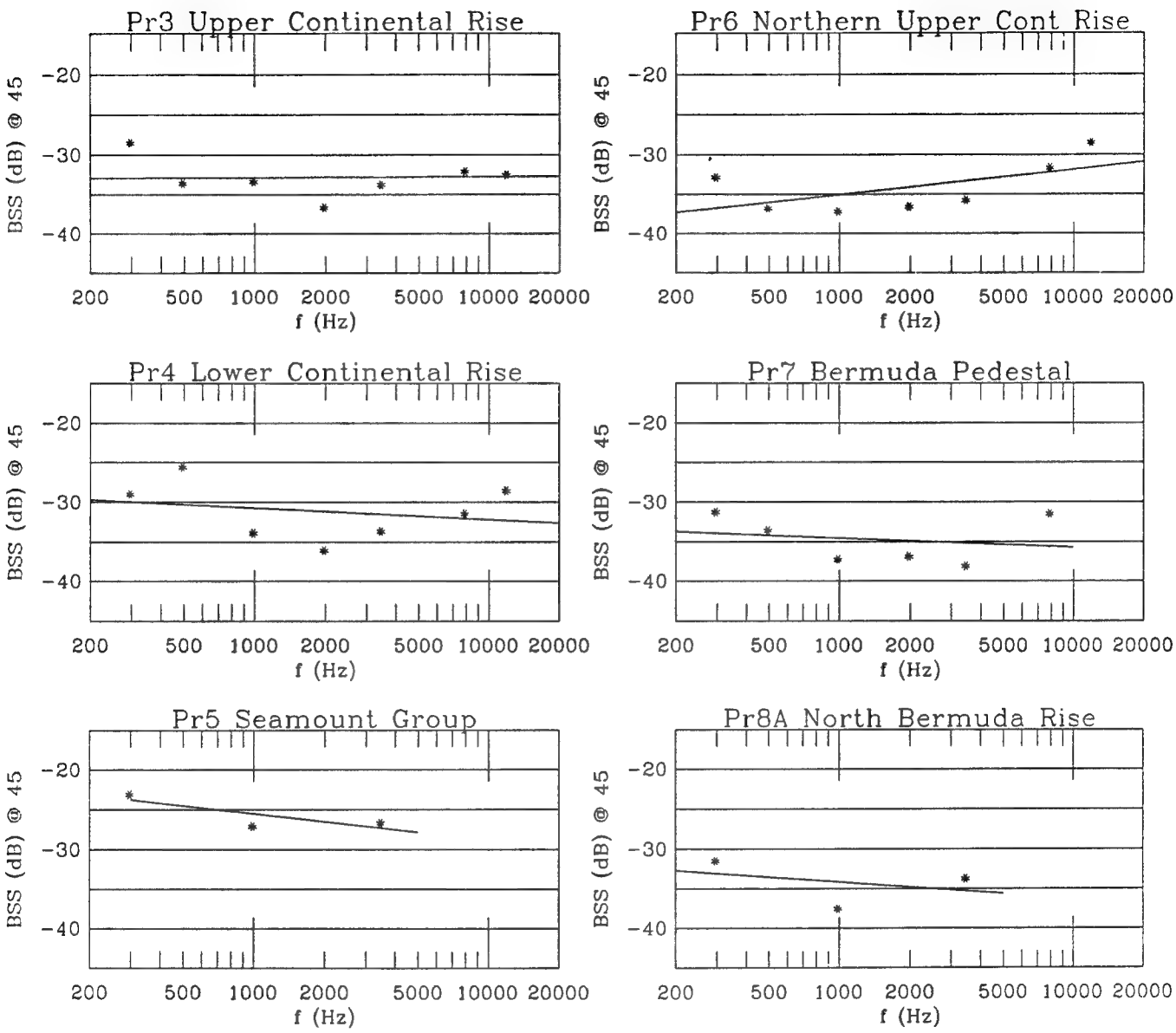

Fig. 9. Compilation of historical bottom backscattering data by Geddes showing frequency dependence at a grazing angle of 45°. The straight lines are regression fits.

Figure 10 compares calculations without and with such an increase in the volume scattering function $\sigma_v(z)$ for the upper layers, and the resulting U-shaped frequency dependence in the latter case. For these calculations, we have chosen the same k^2-linear profile as for Figs. 4 and 5 but have varied the frequency from 100–20,000 Hz. Here the conditions are the same for both the lower and upper curves, except that the upper curve has a 30-cm thick, 15-dB stronger upper layer.

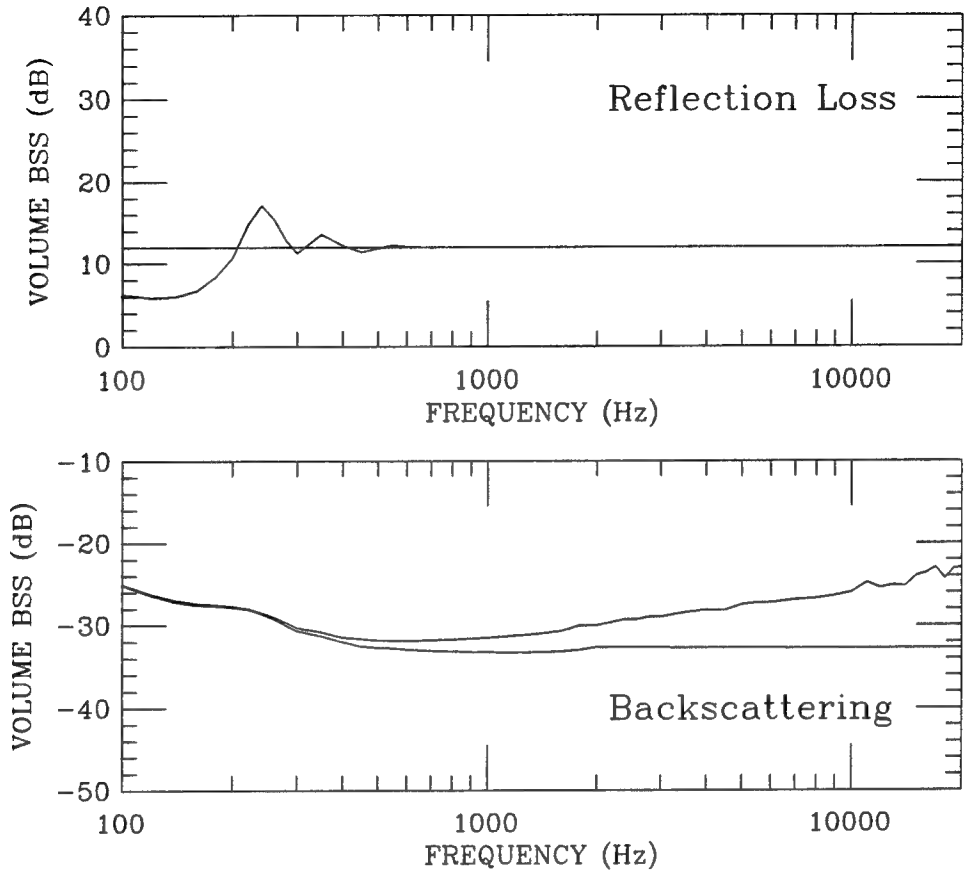

Fig. 10. Model curves showing frequency dependence of reflection loss and backscattering with an upper sediment layer exhibiting strong volume scattering.

A comparison between the layered model and historical data at grazing angles near 45° is made in Fig. 11. The data come from the Lower Continental Rise, which corresponds to Geddes' Province 4. Both Geddes' average of historical data and the DREA data [14] (which are part of the average shown in Fig. 10) are shown in the figure. In the model computation, we assumed that the k^2-linear profile was applicable with the following parameters:

$$\begin{aligned}
\text{Frequency, } f &= 500 \text{ Hz and } 100 \text{ Hz} \\
\text{Water sound speed, } c_w &= 1530.0 \text{ m/s} \\
\text{Surficial sediment sound speed, } c_1 &= 1510.11 \text{ m/s} = c_w \times\ 0.987 \\
\text{Initial slope of sound speed profile, } |dc/dz|_0 &= 1.0 \text{ s}^{-1} \\
\text{Loss parameter, } \delta &= 0.00149 \\
\text{Squared wavenumber, } k^2(z) &= k_1^2\ (1 + i\delta)^2\ (1 - z/z_{\text{wall}}) \\
\text{Real part of surficial wavenumber, } k_1 &= 2\pi f/c_1 \\
\text{Depth of singularity, } z_{\text{wall}} &= -755.1 \text{ m} \\
\text{Mass density, } \rho &= 1.72 \times 1026 \text{ kg/m}^3 \\
\text{Volume scattering parameter, } \sigma_2 &= 0.0003353\ .
\end{aligned}$$

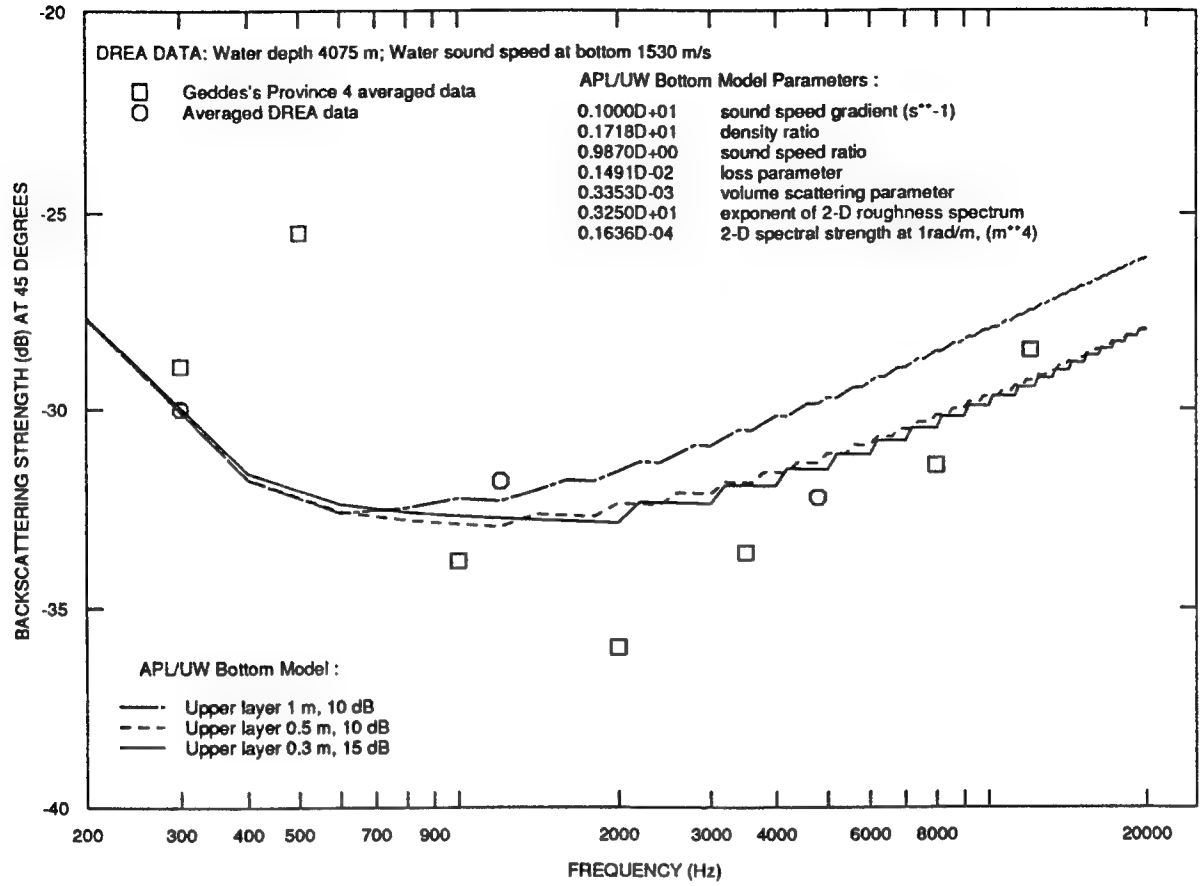

Fig. 11. Comparison of frequency dependence of data from the Lower Continental Rise of the Northeast Atlantic with model curves.

The model input parameters were in part determined from core samples as explained in Ref. [15]. Three different choices were made for the strongly scattering upper layer: (1) a thickness of 1 m and a volume scattering strength that is elevated by 10 dB relative to the value specified above, (2) a thickness of 0.5 m and a volume scattering strength elevated by 10 dB, and (3) a thickness of 0.3 m and a volume scattering strength elevated by 15 dB. The latter two choices give reasonable fits to the data, suggesting a layer of strong scattering that is about 30 cm thick. Comparison of Figs. 10 and 11 shows that the model curve of Fig. 11 is smoother at high frequencies. This is because we employed the Airy function software as in Ref. [1] rather than the numerical propagation code. The propagation code was having numerical difficulty at the highest frequencies, but this was evidently not due to any fundamental limitation of the code, but rather to the fact that the starting point of the integration was taken to be too deep in comparison to the depth of penetration.

3 ROUGHNESS-SCATTERING COMPONENT

The following development is as previously given by Mourad and Jackson [3], except for three changes. The most significant change is a generalization to include the above effects of gradients in sediment properties in the roughness-scattering component of the model. In addition, an algebraic fit to the Kirchhoff integral is abandoned in favor of numerical evaluation of the integral. Finally, the composite-roughness approximation is abandoned in favor of the simpler small-roughness perturbation approach. In the first place, we have found that the particular slope-averaging method used in our earlier models could not deal with the oscillations in scattering strength seen in the present model. Moreover, the difference between the composite-roughness and the small-roughness perturbation approximations was found to be very small at frequencies below 10 kHz. Given the same bottom parameters, the present model will substantially match the the predictions of the older high-frequency model except for very rough, hard bottoms (gravel and rock), where the high-frequency model uses an empirical expression [3]. The present model is inapplicable in these situations.

As in the prior high-frequency model [3], bottom relief is assumed to be a Gaussian random process having the following two-dimensional spectrum:

$$W(\mathbf{K}) = w_2/(Kh_0)^\gamma \ . \tag{17}$$

In this expression, w_2 and γ are model parameters for the strength and exponent of the roughness spectrum, and $h_0 = 1$ m is simply a reference length. Since the roughness spectrum depends only on the magnitude of the two-dimensional wavevector $K = |\mathbf{K}|$, it can be seen that bottom roughness is assumed to be isotropic. The spectrum is defined for both positive and negative arguments and is normalized so that the integral over any finite region of $\mathbf{K}$-space is equal to the mean-square roughness due to those Fourier components included in the integral. Random processes having power-law spectra such as Eq. (17) are fractal without a well-defined correlation scale or rms roughness. Even so, finite and useful results can be obtained provided the exponent satisfies $2 < \gamma < 4$.

The roughness statistics can be alternatively described by the "structure function" [16], itself a power law:

$$< [f(\mathbf{R}_0 + \mathbf{R}) - f(\mathbf{R}_0)]^2 >= C_h^2 R^{2\alpha} \ , \tag{18}$$

where $f(\mathbf{R})$ is the z-coordinate of the interface at horizontal position $\mathbf{R} = (x, y)$. The function $f(\mathbf{R})$ is a zero-mean Gaussian random process. The structure-function parameters are related to the spectrum parameters as follows:

$$\alpha = \frac{\gamma}{2} - 1 \ , \tag{19}$$

and

$$C_h^2 = \frac{2\pi\ w_2\ \Gamma(2-\alpha)\ 2^{-2\alpha}}{h_0^\gamma\ \alpha(1-\alpha)\ \Gamma(1+\alpha)}\ . \tag{20}$$

The roughness scattering component of the backscattering cross section will be written as the sum of two terms:

$$\sigma_{br}(\theta) = \sigma_{kr}\ (\theta)g(x)\ +\ \sigma_{pr}\ (\theta)[1-g(x)]\ . \tag{21}$$

The first term in this equation is computed using the Kirchhoff approximation, and the second is computed using the small-roughness perturbation approximation. The function, $g(x)$, interpolates between these two approximations.

$$g(x) = \frac{1}{1+e^x}\ . \tag{22}$$

The argument of $g(x)$,

$$x = 80\ [\ 0.03\ \sigma_{kr}(\frac{\pi}{2}) - \sigma_{kr}(\theta)\ ]\ , \tag{23}$$

is chosen such that the Kirchhoff approximation is used for angles near vertical incidence and the small-roughness approximation is used for all other angles. Specifically, the Kirchhoff approximation is used from 90°, which is an extremum, down to the angle at which the Kirchhoff cross section has dropped by a factor of 0.03 (about −15 dB) relative to this extremum.

As in Ref. 4, the Kirchhoff cross section will be expressed in the following form:

$$\sigma_{kr}(\theta) = \frac{|R(\pi/2)|^2}{8\pi\ \sin^2\theta\ \cos^2\theta}\int_0^\infty e^{-qu^{2\alpha}} J_0(u)\ u\ du\ , \tag{24}$$

where

$$q = C_h^2\ \sin^2\theta\ \cos^{-2\alpha}\theta\ 2^{1-2\alpha}\ k_w^{2(1-\alpha)}\ . \tag{25}$$

In Eqs. (24) and (25), k_w is the (real) wavenumber in water, $R(\pi/2)$ is the complex plane-wave reflection coefficient for a flat interface separating water and sediment, here evaluated at normal incidence, and $J_0(u)$ is the zeroth-order Bessel function of the first kind.

A significant departure is made from previous versions of the APL-UW bottom backscattering model, in which gradients were ignored and the Rayleigh (or Fresnel) reflection coefficient was used. To account for gradients in the sediment properties, the reflection coefficient, $R(\theta)$, is now computed numerically, as developed in Section 2.2 above, using the profiles for sound speed, density, and absorption coefficient. Equation (24) is also evaluated numerically, as in Ref. 4. This improves upon the algebraic fit to Eq. (24) used by Mourad and Jackson [3]. In this numerical evaluation, we use an algorithm provided by C. deMoustier (private communication).

In the small-roughness approximation, first-order perturbation theory is used to compute scattering from the small-scale roughness of the interface. Following Winebrenner's treatment of the electromagnetic scattering problem, Moe and Jackson [17] have obtained the following expression for the acoustic backscattering cross section of a randomly rough two-fluid boundary:

$$\sigma_{pr}(\theta) = \frac{k_w^4}{4}|1+R(\theta)|^4\, W(2k_w\cos\theta) \times |1-\frac{\kappa^2}{\rho_1}+(1-\frac{1}{\rho_1})\,\cos^2\theta+(\rho_1-1)\,[\frac{1-R(\theta)}{1+R(\theta)}]^2\,\sin^2\theta\,|^2\,. \quad (26)$$

In this equation, ρ_1 is the ratio of sediment density immediately below the interface to water density. Similarly,

$$\kappa = k_1\,(1+i\delta)/k_w \quad (27)$$

is the ratio of the complex wavenumber in the sediment immediately below the interface to the real wavenumber in the water. Expression (26) is a rearrangement of the conventional perturbation-theory result [3, 4, 18]. In this rearrangement the reflection coefficient $R(\theta)$ for the (flat) water/sediment interface appears prominently. The conventional result is recovered if the Rayleigh reflection coefficient is used, and the more general result obtains if the reflection coefficient is computed numerically, including gradients.

Figures 12a and 12b illustrate the effect of sound speed gradients on roughness scattering. The k^2-linear profile is used again, allowing computation of the reflection coefficient in terms of Airy functions. The relevant parameters are

Frequency, f	=	300 Hz, 1000 Hz
Water sound speed, c_w	=	1545.0 m/s
Surficial sediment sound speed, c_1	=	1483.2 m/s $= c_w \times 0.96$
Slope of sound speed profile, $\lvert dc/dz\rvert_0$	=	1.3 s^{-1}
Loss parameter, δ	=	0.0001445
Squared wavenumber, $k^2(z)$	=	$k_1^2\,(1+i\delta)^2\,(1-z/z_{\text{wall}})$
Real part of surficial wavenumber, k_1	=	$2\pi f/c_1$
Depth of singularity, z_{wall}	=	−570.5 m
Mass density, ρ	=	1.548 × 1026 kg/m^3
Volume scattering parameter, σ_2	=	0.0
Spectral exponent, γ	=	3.25
Spectral strength, w_2	=	0.0001636 m^4.

The features of the roughness-scattering component of the scattering strength are similar to those seen for the volume-scattering component. The scattering

strength exhibits strong oscillations, and upward refraction causes an enhancement of the backscattering strength. As in the volume-scattering cases seen earlier, the oscillations and enhancement weaken as frequency increases, owing to absorption which suppresses the upgoing wave. The oscillations show slow variations in strength as a function of grazing angle. This is due to use of composite roughness slope averaging as defined by Mourad and Jackson [3]. Thus the computations leading to Fig. 12 depart slightly from the model defined in this section, in which composite roughness averaging is omitted. The sound-speed profile used here does not contain the type of small-scale structure that would be important at high frequencies. Bioturbation causes strong gradients in sediment acoustic properties on scales of 5–20 cm [5] which could cause upward refraction at high frequencies. The present model provides a means for investigating such effects.

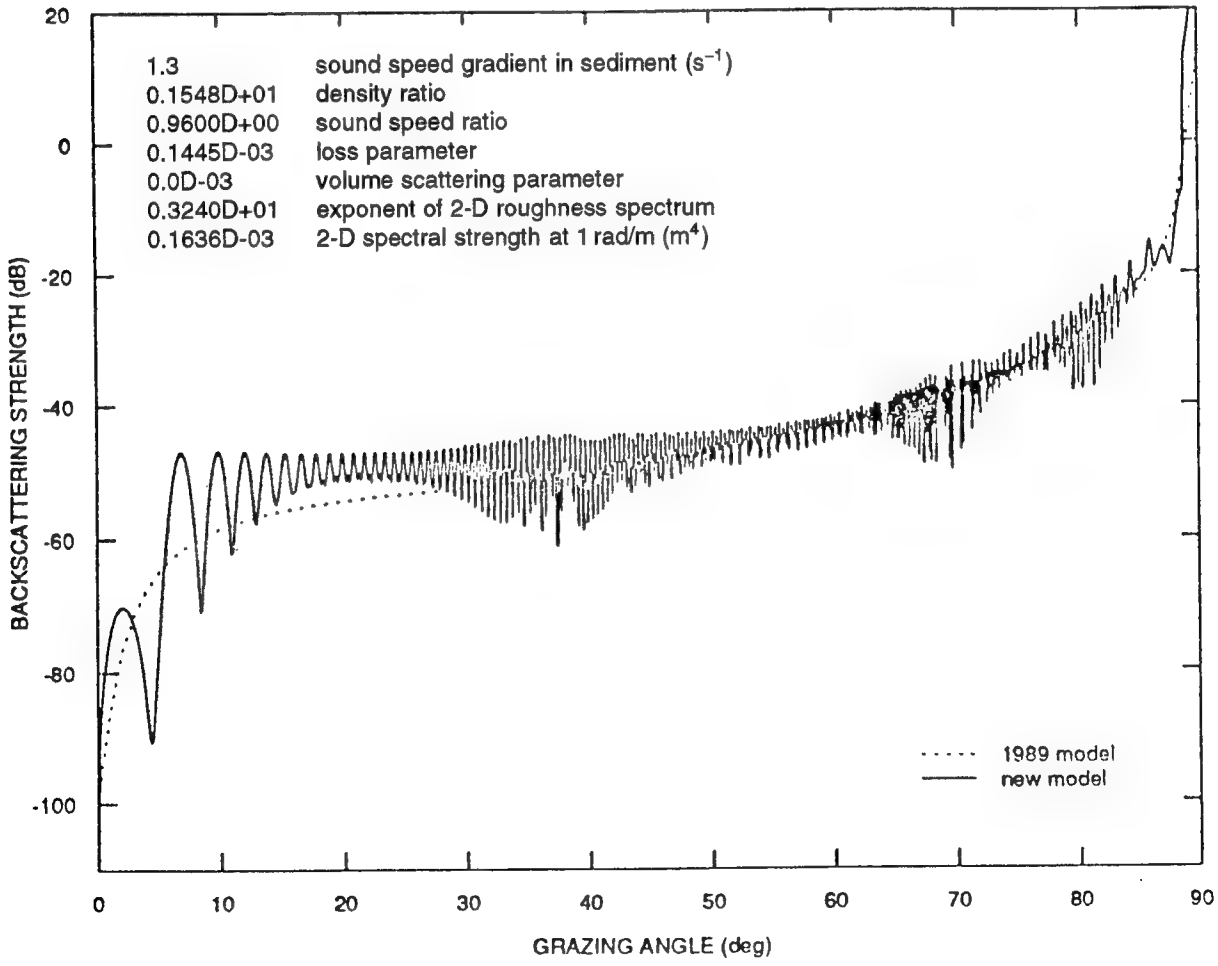

Fig. 12a. Model curves for backscattering strength due to interface roughness with a gradient (solid curve) and without a gradient (dotted curve), 300 Hz.

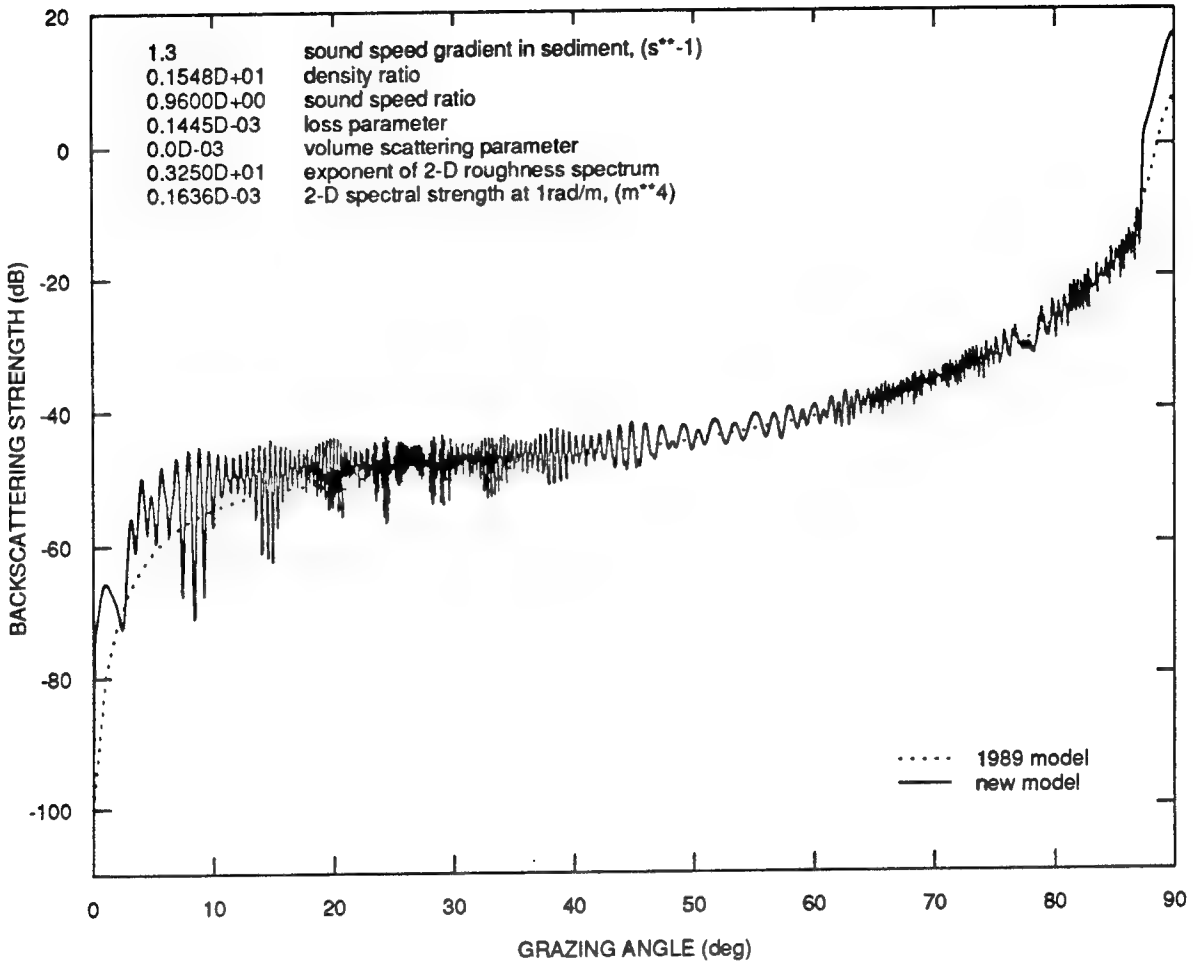

Fig. 12b. Model curves for backscattering strength due to interface roughness with a gradient (solid curve) and without a gradient (dotted curve), 1000 Hz.

4 COMMENTS

Sections 2 and 3 defined the methods for computing the backscattering cross section $\sigma_{bv}(\theta)$, for scattering from sediment volume inhomogeneities, and $\sigma_{br}(\theta)$, for scattering from the rough interface. Bottom backscattering strength BSS is defined as the backscattering cross section per unit area per unit solid angle, expressed in decibels. This is equivalent to the standard definition given by Urick [12]. Combining the two components, we will write the total backscattering strength in the form

$$BSS = S_b(\theta) = 10 \log_{10} [\sigma_{bv}(\theta) + \sigma_{br}(\theta)] . \tag{28}$$

The bottom material is treated as a fluid supporting compressional waves only. Consequently, the sediment properties of interest correspond to those of the APL-UW high-frequency model [3], except that the sediment properties density, sound-speed, absorption, and volume scattering strength are allowed to have general depth profiles.

Earlier models employed dimensionless ratios for sediment properties, and similar normalization may prove convenient in applications of the more general model. For example, sediment mass density and sound speed can be normalized by dividing by the water mass density and water sound speed, c_w, respectively. Although density normalization is mostly a matter of convenience, Hamilton and Bachman [7] argue that the sound speed ratio is an intrinsic property, insensitive to changes in the acoustic properties of the overlying water. Thus, as the sound speed of the water at a given site undergoes changes due to warming, cooling, or changes in salinity, these ratios remain approximately fixed. Therefore, one need change only the water sound speed and the profile for sediment sound speed will automatically adjust to the correct value. The dimensionless parameters already used for absorption loss δ and volume scattering σ_2 represent an attempt to remove the frequency dependence of these parameters. If the user changes the frequency but leaves all other parameters unchanged, the resulting frequency dependence of the model is the default dependence that we expect in most situations. Of course, the user is always free to specify alternate values, including a nondefault frequency dependence.

The two parameters describing bottom roughness are defined in Section 3 and are identical to those employed in past models [2, 3]. In previous versions of this model, the default value $\gamma = 3.25$ was recommended when a measured value is not available. This default value is an average obtained from centimeter-scale bottom roughness spectra obtained by stereophotography [19].

5 CONCLUSIONS AND RECOMMENDATIONS

By generalizing the propagation calculations within a prior model for sediment-volume and interface backscattering, the range of applicability of the model has been greatly increased. More general profiles for sediment acoustic properties now permit the inclusion of small-scale effects such as loosening of the upper sediment by bioturbation and such large-scale effects as consolidation with depth. Although the motivation for the present model was our desire to join earlier models covering disjoint frequency regimes, we went beyond merely interpolating between the two prior models. Our generalized treatment of sediment propagation has introduced new physics, which, in some cases, leads to qualitatively different results. Specifically, we recognize an enhancement in scattering strength relative to the gradient-free case caused by the presence of both upward- and downward-propagating sound in the sediment.

While the model is capable of mimicking the angular and frequency dependence seen in existing backscattering data, it has not been validated owing to a lack of measured physical parameters. There is also a lack of wideband backscattering data spanning low to high frequencies (hundreds of hertz to several kilohertz). In the absence of such data, a first step in bringing the model to a practically useful state is to constrain the sediment profiles based on current geological knowledge and to use the remaining freedom to make empirical fits to existing backscattering data.

Although the present model is well defined mathematically, and we have evaluated it for some nontrivial cases, care was continually required to ensure that particular numerical evaluations always yielded correct results. Other interested workers will have to exercise similar care in their own evaluations of this model. At present we could not supply a user-friendly computer implementation that would relieve users of this responsibility. For our examples, we found it convenient to choose only continuous algebraic profiles of sediment properties. Numerical implementations working from tabular profiles and allowing for discontinuously layered sediments would clearly be desirable as well.

References

[1] P. D. Mourad, P. H. Dahl, and D. R. Jackson, "Bottom backscatter modeling and model/data comparison for 100–1000 Hz," APL-UW TR 9107, Applied Physics Laboratory, University of Washington, September 1991.

[2] P. D. Mourad and D. R. Jackson, "A model/data comparison for low-frequency bottom backscatter," *J. Acoust. Soc. Am.*, **94**, 344–358 (1993).

[3] P. D. Mourad and D. R. Jackson, "High frequency sonar equation models for bottom backscatter and forward loss," *Proceedings OCEANS '89*, 1168–1175 (1989).

[4] D. R. Jackson, D. P. Winebrenner, and A. Ishimaru, "Application of the composite roughness model to high-frequency bottom backscattering," *J. Acoust. Soc. Am.*, **79**, 1410–1422 (1986).

[5] D. R. Jackson and K. B. Briggs, "High-frequency bottom backscattering: Roughness vs. sediment volume scattering," *J. Acoust. Soc. Am.*, **92**, 962–977 (1992).

[6] M. Gensane, "A statistical study of acoustic signals backscattered from the sea bottom," *IEEE J. Oceanic Eng.*, **14**, 84–93 (1989).

[7] E. L. Hamilton and R. T. Bachman, "Sound velocity and related properties of marine sediments," *J. Acoust. Soc. Am.*, **72**, 1891–1904 (1982).

[8] E. L. Hamilton, "Sound velocity-density relations in sea-floor sediments and rocks," *J. Acoust. Soc. Am.*, **63**, 366–377 (1978).

[9] T. Yang and S. L. Broschat, "Acoustic scattering from a fluid-elastic solid interface using the small slope approximation," *J. Acoust. Soc. Am.*, in press.

[10] L. M. Brekhovskikh, *Waves in Layered Media* (Academic, New York, 1960), p. 171.

[11] W. H. Press, B. P. Flannery, S. Teukolsky, and W. T. Vetterling, *Numerical Recipes* (Cambridge University Press, Cambridge, MA, 1986) pp. 495–97 ?.

[12] R. J. Urick, *Principles of Underwater Sound*, 3rd Ed. (Mc-Graw Hill, New York, 1983).

[13] R. E. Christenson, J. A. Frank, and W. H. Geddes, "Low-frequency propagation via shallow refracted paths through deep ocean unconsolidated sediments," *J. Acoust. Soc. Am.*, **57**, 1421–1426 (1975).

[14] W. H. Geddes, "Least square fit of Lambert's law to bottom backscatter measurements in the North Atlantic test area," GGAI Tech. Note 3-92, Geddes Geophysical Associates, Inc., Long Beach, Mississippi, 1992.

[15] K.-Y. Moravan and D. R. Jackson, "Model/Data Comparison for Bottom Backscatter in the North Atlantic at Low Frequencies," APL-UW TR 9304, Applied Physics Laboratory, University of Washington, February 1993.

[16] A. M. Yaglom, *An Introduction to the Theory of Stationary Random Functions*, (Prentice-Hall, Englewood Cliffs, N.J., 1962).

[17] J. E. Moe and D. R. Jackson, "First-order perturbation theory for rough surface scattering cross section of a fluid-fluid interface including the effect of gradients," *J. Acoust. Soc. Am.*, in press.

[18] E. Y. Kuo, "Wave scattering and transmission at irregular surfaces," *J. Acoust. Soc. Am.*, **36**, 2135–2142 (1964).

[19] K. B. Briggs, "Microtopographical roughness of shallow-water continental shelves," *IEEE J. Oceanic Eng.*, **14**, 360–367 (1989).

REPORT DOCUMENTATION PAGE

Form Approved
OPM No. 0704-0188

1. AGENCY USE ONLY *(Leave blank)*	2. REPORT DATE	3. REPORT TYPE AND DATES COVERED
	April 1994	Technical

4. TITLE AND SUBTITLE

100 Hz–10 kHz Bottom Backscattering Model: Generalized Treatment of Sediment Sound Propagation, Sediment Volume Scattering, and Interface-Roughness Scattering

5. FUNDING NUMBERS

N00039-91-C-0072

6. AUTHOR(S)

Darrell R. Jackson, Paul D. Ingalls, and Kou-Ying Moravan

7. PERFORMING ORGANIZATION NAME(S) AND ADDRESS(ES)

Applied Physics Laboratory
University of Washington
1013 NE 40th Street
Seattle, WA 98105-6698

8. PERFORMING ORGANIZATION REPORT NUMBER

APL-UW TM 1-94

9. SPONSORING / MONITORING AGENCY NAME(S) AND ADDRESS(ES)

Office of Naval Research
800 N. Quincy Street
Arlington, VA 22217

10. SPONSORING / MONITORING AGENCY REPORT NUMBER

11. SUPPLEMENTARY NOTES

12a. DISTRIBUTION / AVAILABILITY STATEMENT

Approved for Public Release; Distribution Unlimited

12b. DISTRIBUTION CODE

13. ABSTRACT *(Maximum 200 words)*

A model for bottom backscattering strength in the frequency range 100 Hz to 10 kHz is presented. This model generalizes an earlier low-frequency model intended for the smaller frequency range 100–1000 Hz. The new model matches the predictions of an existing high-frequency model (10–100 kHz) but offers new insights into the effect of fine-scale layering. Scattering from both sediment volume inhomogeneity and interface roughness is included in the model. For silt and clay sediments, sediment volume scattering is usually the dominant process. The model requires profile functions for average sound speed, mass density, sound absorption, and volume scattering strength in the sediment. In addition, two parameters describing the spectrum of interface roughness are required. Use of the small-roughness perturbation approximation prevents application of the model to extremely rough bottoms (e.g., gravel and rock).

Preliminary comparisons with data show that the model can reproduce an interesting frequency dependence often seen in bottom backscattering. This includes a decrease in scattering strength with increasing frequency in the 100–1000 Hz range, an increase as frequency approaches 10 kHz, and approximate constancy or a slow rise above 10 kHz. The increase in sound speed with depth typically observed in sediments causes upward refraction which, in some cases, leads to enhancements of scattering by 6–8 dB.

14. SUBJECT TERMS	15. NUMBER OF PAGES
Bottom backscattering, sediment sound propagation, sediment volume scattering, interface roughness scattering	33
	16. PRICE CODE

17. SECURITY CLASSIFICATION OF REPORT	18. SECURITY CLASSIFICATION OF THIS PAGE	19. SECURITY CLASSIFICATION OF ABSTRACT	20. LIMITATION OF ABSTRACT
Unclassified	Unclassified	Unclassified	SAR